Sub-THz Switch-less Reconfigurable Triple-/Push-push Dual-band VCO for 6G Communication

Seongwoog Oh, Jinhyun Kim, Jungsuek Oh
Institute of New Media and Communications (INMC) and Department of Electrical and Computer Engineering, Seoul National University, South Korea
{dillon1859, jinhyun111, jungsuek}@snu.ac.kr

***Abstract*— This work presents a novel switch-less reconfigurable triple-/push-push dual-band VCO topology and design methods for a W-band metal–oxide–semiconductor (CMOS) voltage-controlled oscillator (VCO). A clover-shaped inductor with a three-port connection and single frequency multiplied output port configuration provides switch-less mode changes between triple-push and push-push operation. This topology is demonstrated in a W-band VCO by controlling three cores with a measured phase noise of -109.17 dBc/Hz at a 10-MHz offset of a 105.3 GHz carrier. The measured center frequency of each band is 91.04 GHz and 102.33 GHz with a tuning range of 10.4% and 14.1%, respectively. The proposed VCO with independent core on/off state control enables low parasitic switch-less frequency band shift resulting in a superior tuning range compared to those of conventional dual-/single-band VCOs. The effectiveness of this approach is demonstrated through fabrication in a 28-nm CMOS process, with the best FOM$_T$ being -174.4 dBc/Hz in this case.**

***Keywords*— dual-band, reconfigurable oscillator, sub terahertz, switch-less, voltage-controlled oscillator.**

I. Introduction

For the sixth generation (6G) of mobile communications, which is expected to be commercialized around 2030, communication systems on the sub-terahertz (sub-THz) frequency band are being studied to meet the requirements of high data rates [1]. There are issues related to the targeting of such a wide frequency range with a single-band voltage-controlled oscillator (VCO) due to bandwidth limitations. At present, multi-band VCOs are often used to overcome these limitations in multi-function transmit/receive architectures such as communication systems. Prior works utilize inductors combined with switches [2], transformers [3], and filtering techniques [4] for dual-band operation in VCOs. A switch loaded directly onto the VCO core acts as the major limiting factor of the passive quality factor (Q) of the resonator, and the deterioration effect becomes more significant as the frequency increases to the sub-THz band ranges. When switching the resonator by utilizing inductive coupling based on the transformer, Q-factor reduction due to the switch can be mitigated. However, transformers inherently have a lower Q-factor than inductors that constitute the same inductance, and they have a trade-off relationship between the coupling coefficient and the self-resonant frequency, which still makes it difficult to use a switch dual-band VCO. A switch-less resonator based on a dual-band filter is not affected by the limiting of the Q-factor, making this topology suitable for use below 5 GHz. Above millimeter-wave frequencies, the VCO performance is limited due to the on-chip filter with a low Q-factor, and multiple inductive components are used to implement multi-resonance, which occupies a large chip area.

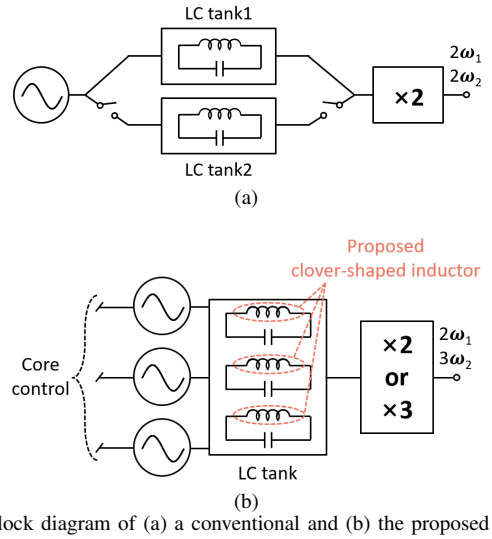

Fig. 1. Block diagram of (a) a conventional and (b) the proposed dual-band W-band VCO.

In complementary metal–oxide–semiconductor (CMOS) VCOs over the W-band, harmonic oscillation strategies such as push-push or tripling techniques are used rather than the fundamental frequency due to an oscillation start-up issue caused by the low Q-factor of the varactor-based resonator and the low gain of the metal oxide semiconductor field-effect transistor (MOSFET) [5], [6]. A conventional block diagram of a W-band VCO with the switching dual-band technique is shown in Fig. 1a. A controlled resonator based on a switch cannot escape from the low Q-factor issue as it must target the millimeter-wave band even when using a push-push topology. In this study, a configuration using three oscillating cores with a clover-shaped inductor is proposed, as shown in Fig. 1b. By controlling the cores, triple-push and push-push reconfigurable operations are achieved to implement a switch-less dual-band VCO operating on the W-band.

II. Switch-less Reconfigurable Dual-band VCO

A. Clover-shaped Inductor Design

The structure of the proposed clover-shaped inductor is shown in Fig. 2. Three single-loop inductor structures

2022 IEEE Radio Frequency Integrated Circuits Symposium (RFIC) | 978-1-6654-9611-7/22/$31.00 ©2022 IEEE | DOI: 10.1109/RFIC54546.2022.9863159

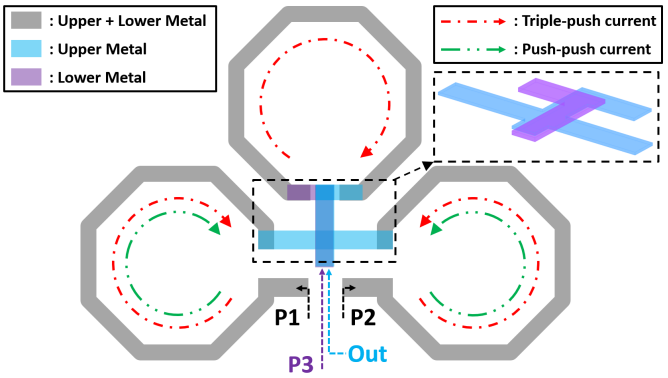

Fig. 2. Top view of the proposed clover-shaped inductor with triple-/push-push current paths.

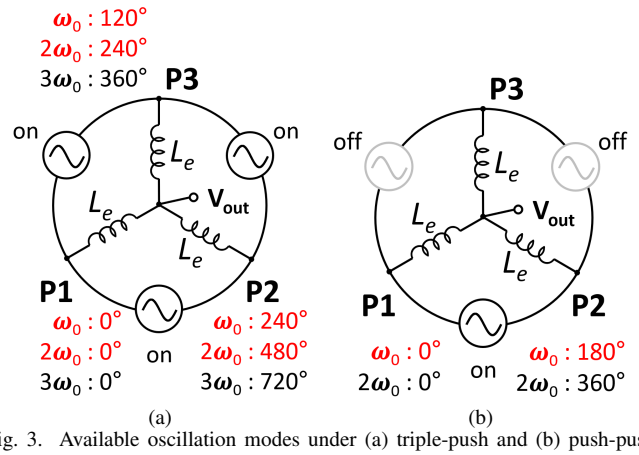

Fig. 3. Available oscillation modes under (a) triple-push and (b) push-push operation when cores are controlled.

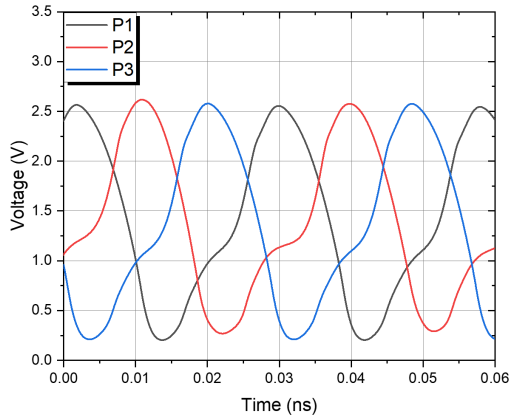

Fig. 4. Simulated voltage waveform at each node of the inductor for triple-push operation.

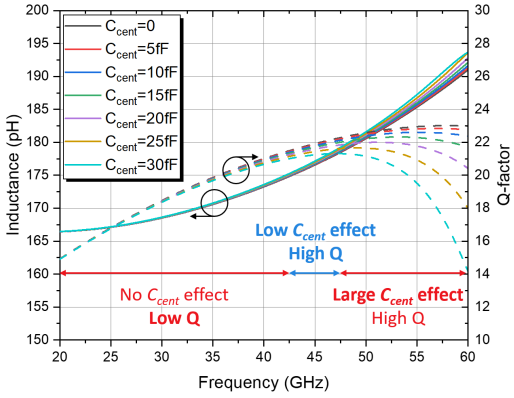

Fig. 5. Simulated results of the C_{cent} effect on the inductance and Q-factor during push-push operation.

with two metal layers (upper and lower) are arranged in a clover shape, and one end of each loop is connected using metal at the upper part, which is the output port where the frequency-tripled or -doubled signal is formed. The ends that are not connected to the other loops are configured as P1, P2, and P3. The corresponding ports are respectively connected to different oscillation cores. When all cores are controlled under operation, the current flowing through the clover-shaped inductor follows a triple-push current path. The detailed triple-push operation considering the current path of the inductor is shown in Fig. 3a. Because there is a 120-degree phase difference between each port at the oscillating fundamental frequency of ω_0, only the $3\omega_0$ signal is added at V_{out} while the other harmonics are canceled. As described in Fig. 3b, when the single core located between P1 and P2 is turned on while the other two are off, the current flowing through the inductor follows the push-push current path. Given that P3 becomes a floating node due to deactivated cores, the V_{out} node is equivalently connected to the center tap of an inductor in a differential mode, which performs the push-push operation.

Fig. 4 shows the simulated voltage waveform at each inductor node when operating in the triple-push mode. Because the relative voltage phase difference of each inductor port connected to the core is approximately 120 degrees, the VCO will result in a triple-push operation as depicted in Fig. 3a. When the VCO operates with rail-to-rail voltage swing, the voltage, including higher harmonics, is given by

$$V(\omega_0) = A_0(sin(\omega_0 t) + v_2 sin(2\omega_0 t) + v_3 sin(3\omega_0 t)) \quad (1)$$

where A_0, v_2, and v_3 denote the amplitude and the relative voltage of the second and third harmonics compared to the fundamental signal, respectively. Higher-order harmonics above the fourth order are ignored considering the f_T of the MOSFET and for simplicity of the analysis. Through the Fourier transform, it can be seen that v_2 and v_3 of the simulated voltage are -0.5 and 0.25, respectively. Given that the third harmonics are summed in-phase at the V_{out} node, the frequency tripled output has 0.75 times the magnitude of the fundamental frequency voltage oscillating at the core.

When the VCO is in push-push operation, the V_{out} node is loaded with a series LC consisting of an inductor connected to P3 (L_e) and a parasitic capacitor (C_{cent}). As shown in Fig. 5, the characteristics of the inductor connected to P1 and P2 are changed by C_{cent}, which is the sum of the varactor and the off-core parasitic capacitance. Although the characteristic change can be neglected in the low-frequency band (<42.5 GHz), the Q-factor of the inductor is low. In the high-frequency

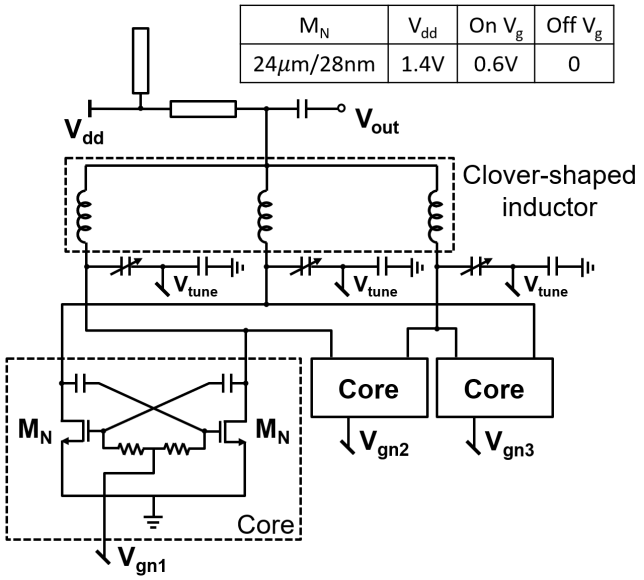

Fig. 6. Schematic of W-band switch-less reconfigurable dual-band VCO consisting of three cores and clover-shaped inductor.

band (>47.5 GHz), the Q-factor is reduced by 39% due to the C_{cent} effect. The frequency of 45 GHz is selected as the VCO target fundamental frequency due to the difference in the Q-factor with the maximum being only 1, and the C_{cent} degradation effect remains within 5%.

B. *Voltage-controlled Oscillator Design*

Fig. 6 presents a schematic illustration of the proposed W-band switch-less reconfigurable dual-band VCO. Each core is based on a cross-coupled structure composed of M_N pairs to generate negative transconductance with capacitive feedback to apply the gate voltage independently for on/off control. Through a bias-T circuit, V_{dd} is applied to a clover-shaped inductor output node where a tripled or doubled signal is formed. The LC tank consists of a clover-shaped inductor, and three varactors connected to a DC block are loaded on each inductor port. If a pair of varactors is connected between each port as a typical cross-coupled VCO, a virtual ground is not guaranteed in the middle of the pair for triple-push operation. Thus, a current path is formed through the varactors from one port to another, creating an additional unintended resistance component. The reconfigurable dual-band oscillation of the VCO is controlled by the gate voltage applied to each core. The triple-push operation is configured when 0.6 V is applied to the gates of all cores. For push-push operation, only V_{gn1} is 0.6 V, while 0 V is applied to the remaining cores to ensure that the cores remain off. Because there is no switch connected to the VCO oscillation node, the possible parasitic capacitance can be minimized. Therefore, the proposed dual-band VCO is capable of frequency tuning range performance comparable to that of the single-band topology.

III. Measurement Results

As a proof of concept, the VCO is fabricated in the Samsung 28-nm CMOS process with an active core size of 0.19 mm × 0.18 mm. A micrograph of the chip is shown in Fig. 7. The measurement of the prototype VCO was performed under on-wafer probing using a Cascade infinity ground-signal-ground I110 probe. The oscillation frequency and phase noise are measured using an Agilent E4448 spectrum analyzer with an Agilent 11970W W-band harmonic mixer.

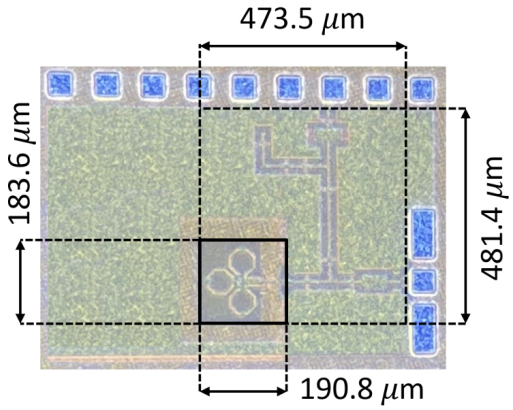

Fig. 7. Chip micrograph of the proposed dual-band VCO.

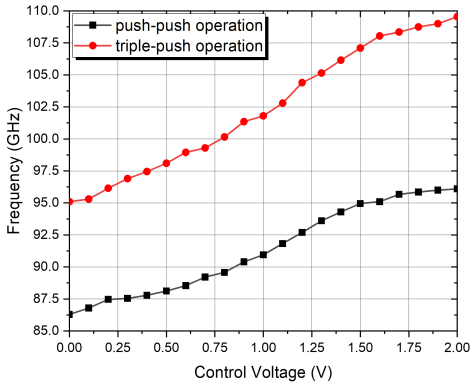

Fig. 8. Measured frequency tuning range of the dual-band VCO.

Fig. 8 shows the frequency tuning range as measured through a varactor control process with a 1.4 V supply voltage, consuming 21.21 and 62.23 mW for push-push and triple-push operations, respectively. The triple-/push-push operation for band shifting is determined by the core on/off state, as presented in Section II-B. With a change in the control voltage, the measured tuning ranges for push-push and triple-push operations are 86.29–95.79 GHz and 95.1–109.55 GHz, respectively. The frequency overlap between the two bands is designed in consideration of the frequency shift due to the error caused by the process and temperature. The proposed dual-band VCO achieves a band overlap of 690 MHz employing control voltage in the range of 0–2 V. Fig. 9 shows the measured phase noise at 105.3 GHz when operating in the triple-push mode. The phase noise outcomes at 1MHz and 10MHz offsets are correspondingly -83.17 dBc/Hz and -109.17 dBc/Hz.

The measured dual-band VCO performance capabilities are summarized and compared with those of state-of-the-art

Table 1. Performance comparison of dual-band VCOs in W-band implemented using CMOS technology.

	This work	**ISIC [7]**†	**RFIC [8]**	**RFIT [5]**	**MWCL [6]**	**TMTT [9]**
Technology	28nm CMOS	65nm CMOS	28nm CMOS	90nm CMOS	90nm CMOS	65nm CMOS
Topology	Push-/triple-push dual-band VCO	Fundamental dual-band VCO	Fundamental dual-band VCO	Push-push single VCO	Tripling single VCO	Fundamental single VCO
Frequency (GHz))	91.04 / 102.33	76.8 / 79.25	73.75 / 88.15	90.1	82.65	89.4
FTR (%)	10.4 / 14.1	1.04 / 1.89	6.37 / 5.79	2.24	15.61	5.15
PN@1MHz (dBc/Hz)	-83.17	-90.8	-93.5 / -86.2	-83.52	-87.9	-81.5
PN@10MHz (dBc/Hz)	-109.17	-113.3	-117.7 / -110.0	-109.22	-	-108.3
P_{DC} (mW)	21.21 / 62.23	30	35.6	25.43	62.4	11
FoM (dBc/Hz)*	-171.4	-176.6	-179.4 / -173.4	-174.3	-168.3	-176.9
FoM_T (dBc/Hz)**	-174.4	-162.1	-175.6 / -168.6	-161.3	-172.2	-171.1
Size (mm^2)	0.035	0.032	0.031	0.31‡	1.3	0.013

*: $FoM = L(\Delta f) - 20\log(f_{osc}/\Delta f) + 10\log(P_{DC}/1mW)$; **: $FoM_T = FoM - 20\log(10 \cdot FTR)$
† : Simulation results; ‡: Pad included.

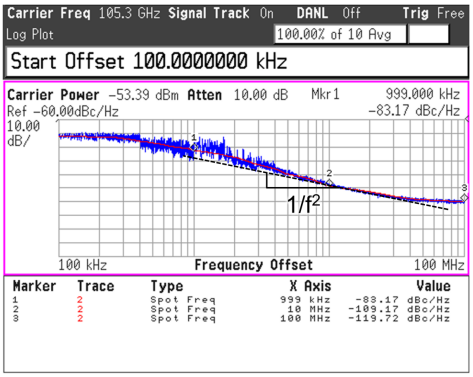

Fig. 9. Phase noise measurement result at 105.3 GHz.

integrated VCO circuits operating on the W-band in Table 1. The phase noise figure-of-merit (FoM) and FoM_T with phase noise and the frequency tuning range (FTR) are used for comparison. The proposed topology shows superior FoM_T outcomes relative to solutions based on fundamental oscillation with a small chip area. To the best of the authors' knowledge, a switch-less dual-band VCO is proposed for the first time with performance comparable to those of the state-of-the-art W-band VCOs in silicon.

IV. Conclusion

A W-band switch-less reconfigurable triple-/push-push dual-band VCO in 28 nm CMOS technology is demonstrated. The VCO design is carried out with three cores providing negative transconductances combined with the proposed clover-shaped inductor that formed a structure of three ports for core connection and a multiplied frequency output port. The proposed topology enables reconfigurable oscillation-band control without loading switches in the RF path. The measured VCO achieves a FoM_T value of -174.4 dBc/Hz at 105.3 GHz occupying an area of 0.035 mm^2.

Acknowledgment

This work was supported by Institute of Information & communications Technology Planning & Evaluation (IITP) grant funded by the Korea government (MSIT) (No.2021-0-00763, Innovative Fusion Technologies of Intelligent Antenna Material/Structure/Network for THz 6G) and Samsung Electronics (Development of Dualband/Wide-band High Efficiency Power Amplifier MMIC for 5G Applications). The chip fabrication and EDA tool were supported by the IC Design Education Center (IDEC), Korea.

References

[1] W. Saad, M. Bennis, and M. Chen, "A vision of 6g wireless systems: Applications, trends, technologies, and open research problems," *IEEE Netw.*, vol. 34, no. 3, pp. 134–142, May/June 2020.

[2] E. Mammei, E. Monaco, A. Mazzanti, and F. Svelto, "A 33.6-to-46.2ghz 32nm cmos vco with 177.5dbc/hz minimum noise fom using inductor splitting for tuning extension," in *Proc. 2013 IEEE Int. Solid-State Circuits Conf. (ISSCC) Dig. Tech. Papers*, San Francisco, USA, Feb. 2013, pp. 350–351.

[3] S. Oh, K.-S. Seo, and J. Oh, "Low phase noise concurrent dual-band (5/7 ghz) cmos vco using gate feedback on nonuniformly wound transformer," *IEEE Microw. Wireless Compon. Lett.*, vol. 31, no. 2, pp. 177–180, Feb. 2021.

[4] B. Li, Y. Liu, C. Yu, and Y. Wu, "Independent control function for concurrent dual-band vco," *IEEE Microw. Wireless Compon. Lett.*, vol. 28, no. 3, pp. 230–232, Mar. 2018.

[5] S.-H. Liu, C.-M. Hung, H.-R. Chuang, and T.-H. Huang, "A w-band push-push vco with gm-boosted colpitts topology in 90-nm cmos technology," in *Proc. 2021 IEEE Int. Symp. Radio-Frequency Integration Technology (RFIT)*, Hualien, Taiwan, Aug. 2021, pp. 1–3.

[6] K.-W. Tan, T.-S. Chu, and S. S. H. Hsu, "A 76.2–89.1 ghz phase-locked loop with 15.6% tuning range in 90 nm cmos for w-band applications," *IEEE Microw. Wireless Compon. Lett.*, vol. 25, no. 8, pp. 538–540, Jun. 2015.

[7] J. Lee, Y. Moon, and T. Ahn, "A dual-band vco using inductor splitting for automotive radar system at w-band," in *Proc. 2014 Int. Symp. Integrated Circuits (ISIC)*, Singapore, Feb. 2014, pp. 168–171.

[8] M. Vigilante and P. Reynaert, "A dual-band e-band quadrature vco with switched coupled transformers in 28nm hpm bulk cmos," in *Proc. 2015 IEEE Radio Frequency Integrated Circuits (RFIC) Symp.*, Phoenix, USA, May 2015, pp. 119–122.

[9] T. Xi, S. Guo, P. Gui, D. Huang, Y. Fan, and M. Morgan, "Low-phase-noise 54-ghz transformer-coupled quadrature vco and 76-/90-ghz vcos in 65-nm cmos," *IEEE Trans. Microw. Theory Techn.*, vol. 64, no. 7, pp. 2091–2103, Jun. 2016.